Published in: Coloma Ribera *et al.* Journal of Applied Physics **118** (5), 055303 (2015)
http://dx.doi.org/10.1063/1.4928295

Determination of oxygen diffusion kinetics during thin film ruthenium oxidation

R. Coloma Ribera,[1,a)] R.W.E. van de Kruijs,[1] A. E. Yakshin,[1] and F. Bijkerk[1]

[1]MESA+ Institute for Nanotechnology, University of Twente, P.O. Box 217, 7500 AE Enschede, The Netherlands.

Abstract:

In situ X-ray reflectivity was used to reveal oxygen diffusion kinetics for thermal oxidation of polycrystalline ruthenium thin films and accurate determination of activation energies for this process. Diffusion rates in nanometer thin RuO_2 films were found to show Arrhenius behaviour. However a gradual decrease in diffusion rates was observed with oxide growth, with the activation energy increasing from about 2.1 to 2.4 eV. Further exploration of the Arrhenius pre-exponential factor for diffusion process revealed that oxidation of polycrystalline ruthenium joins the class of materials that obey the Meyer-Neldel rule.

Keywords: diffusion rates, activation energies, oxygen diffusion, ruthenium oxide, thin films, X-ray reflectivity

I. INTRODUCTION

Ruthenium oxide (RuO_2) presents several attractive properties such as low resistivity,[1] high thermal stability,[2] good diffusion barrier capability,[3] excellent catalytic performance,[4,5] and easy patterning.[6] These interesting properties can make RuO_2 a suitable candidate for a large number of applications. For instance, RuO_2 can be used as oxidation catalyst in heterogeneous catalysis and electrocatalysis,[7] as bottom gate electrode of oxide dielectric capacitors in dynamic random access memories (DRAMs),[8] or as protective capping layer in extreme ultraviolet lithography (EUVL).[9,10,11] In the last two applications, oxygen diffusion towards deeper layers is known to be one of the main threats for functionality. The fabrication of high-K dielectric capacitors is performed at high temperatures and in an oxidative environment. Under such extreme conditions, the poly-Si plug attached to the gate electrode can be oxidized with a subsequent dielectric thickness increase, which then results in a marked reduction of the effective dielectric constant of the capacitor with negative implications for its performance.[8] Under EUV radiation, the cracking of water vapour potentially present in the system will induce oxidation of the Si/Mo multilayer mirrors resulting in a drop in reflectivity with a consequently decrease of the optics lifetime.[10,12] In both cases, a protection barrier for oxygen diffusion is necessary, for which RuO_2 has been considered as a good candidate. However, there is a lack of knowledge on diffusion kinetics, diffusion constants and activation energies for oxygen diffusion in RuO_2 thin films that would allow determination of the degradation rate of the structures due to oxidation.

[a)] Author to whom correspondence should be addressed. Electronic mail: r.colomaribera@utwente.nl

The limited availability of data on diffusion constants in nanometer thin films is due to the very intricate measurement of diffusion coefficients in systems with short diffusion lengths.[13] The commonly used techniques for this purpose, such as transmission electron microscopy and X-ray photoelectron spectroscopy, do not allow to determine small changes in the structures with sufficient precision. To tackle this problem, in our recent work,[14] *in situ* hard X-ray reflectivity measurements were used for monitoring thermal oxidation of Ru thin films. This allowed accurate determination of the changes of the in-depth electron density distribution during the thin film growth. There, we reported about co-existence of 3D surface and 2D sub-surface oxidation. In this study, we focus on the determination of diffusion kinetics for the sub-surface oxidation process of Ru thin films. Diffusion rates and activation energies for oxygen diffusion through a few nanometer thick ruthenium oxide layers have been accurately determined.

II. EXPERIMENTAL

Ten nanometer thick polycrystalline Ru films were deposited by DC magnetron sputtering at room temperature onto natively oxidized super-polished Si substrates in an UHV setup with base pressure $<1 \times 10^{-8}$ mbar. To prevent intermixing of Ru and Si during annealing, and resulting complications in X-ray reflectivity data analysis, a 15 nm SiO_2 diffusion barrier was deposited on top of the Si wafer before Ru deposition. All layer thicknesses were monitored using quartz mass balances and used as initial fit parameters for XRR analysis.

In situ monitoring of Ru oxidation during annealing was conducted with X-ray reflectivity (XRR) measurement using a PANalytical Empyrean X-ray diffractometer (Cu-Kα radiation, 0.154 nm), equipped with an Anton Paar thermal stage.[15] Before annealing, the sample position was aligned with respect to the impinging X-ray beam and a reference XRR spectrum was recorded. Then, the sample was heated to a predefined temperature and a sample realignment was carried out to correct for thermal expansion and possible misalignment. Subsequently, XRR scans were repeatedly performed during annealing.

The deposited Ru films were annealed at different temperatures for different amounts of time depending on temperature. GenX software was used for XRR data analysis.[16] A layered model of the structure was simulated using GenX, and the thickness, roughness and density of each of the layers in the model were varied using a genetic algorithm in order to minimize the differences between model simulations and experimental data. Layer thicknesses and densities were determined with accuracies of ±0.1 nm and $\pm 0.3\ g \cdot cm^{-3}$, respectively. Ruthenium oxide thicknesses were monitored in time to obtain diffusion constants and activation energies.

X-ray diffraction (XRD) patterns were also recorded using a PANalytical Empyrean X-ray diffractometer (Cu-Kα radiation, 0.154 nm).

III. RESULTS AND DISCUSSION

Fig. 1 presents an example of the measured and simulated XRR data for (a) an as deposited and (b) annealed sample at 400°C for 20 minutes. The models consisted of a Si substrate, a SiO_2 layer, a Ru layer and one or two RuO_2 layers, as shown in the insets of Fig.1.

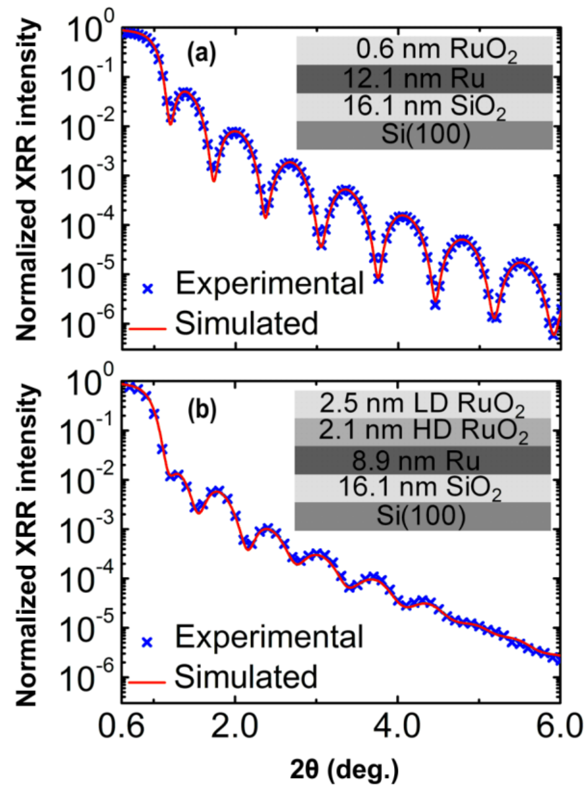

FIG. 1. (Color online) Experimental (crosses) and simulated (line) specular X-ray reflectivity data for (a) an as deposited sample and (b) a sample annealed at 400°C for 20 min. Top-right (a) and (b) insets show the layered models used for each simulation. LD ($0.7\rho_{bulk}$) and HD (ρ_{bulk}) denote low and high density, respectively.

The XRR data for the as deposited sample could be modelled using a single thin surface oxide layer with a density of 6.0±0.3 g·cm^{-3} which is somewhat lower than the bulk density of RuO_2, 6.8 g·cm^{-3}. The structure model is depicted in Fig. 1(a). In the range of temperatures from 150 to 350°C the oxide layer thickness increased from 0.7±0.1 to 2.4±0.1 nm, respectively, with the density being 6.0±0.3 g·cm^{-3}. Above about 350°C, however, XRR data could not be modelled anymore by a single surface oxide layer. To find an appropriate model for the oxide, a test model was created. For a sample annealed during 12 h at 400°C, the oxide layer was subdivided into 9 thinner oxide layers of 1 nm each, with the density for each sub-layer being varied by the genetic algorithm from 5 to 7.5 g·cm^{-3}. The other layers remained as in the initial model and were fitted in the conventional way. The result of the fit showed a clear separation of the oxide into two parts. The top three sub-layers had consistently lower density of about 70% compared to the bottom six sub-layers having close to the bulk RuO_2 density. So above 350°C it was necessary to use a 2-layer instead of 1-layer

oxide model to better describe the oxidation process, a low density (LD) RuO_2 layer on top of a high density (HD) RuO_2 layer, with LD and HD oxide densities being 5.3±0.3 and 6.8±0.3 g·cm^{-3}, respectively (see (Fig. 1(b)). The low density RuO_2 quickly saturated with annealing time at a thickness of about 3 nm while the high density RuO_2 continued to grow as shown by the open and closed symbols in Fig. 2(a), respectively. Note that the reason for the origin of the low density oxide is not clear and needs further investigation. But since the high density RuO_2 was the only growing oxide species, the oxygen diffusion kinetics was studied monitoring the thickness of this layer.

For this study the temperatures had to be carefully selected. First of all only above 350°C XRR analysis suggested formation of close to bulk density RuO_2.At the same time the temperatures higher than 400°C provoked strong surface morphology changes, observed by the drop of the XRR signal, probably due to the pronounced formation of surface nano-columns.[14] Such morphology changes strongly reduce the apparent optical contrast in the XRR, which lowers accuracy of XRR analysis. For this reason *in situ* XRR measurements during annealing were done in the carefully selected range of temperatures, at 380, 390, and 400°C. The small range of temperatures and the increment of only 10 degrees insured minimum possible structural differences in the growing oxides at different temperatures. Resolving changes in diffusion rates with this small increment in temperature became possible due to the high accuracy of the oxide thickness determination with XRR measurements. Furthermore, before the experiment the samples were pre-annealed at 400°C for 2 h. At this step the low density oxide layer is saturated at a thickness of approximately 3 nm and there is a layer of about 2.8 nm near bulk RuO_2 formed (see Fig. 2(a)). The pre-annealing step allowed us to avoid a non diffusion limited or concentration dependent diffusion processes that shortly occur at the initial stage of surface oxidation which also strongly depend on the temperature of annealing.

To exclude a possible effect of changing structure with time for different temperatures, diffusion rates were determined at fixed oxide thicknesses, rather than fixed annealing time, for different temperatures. So here initially an assumption was made that for every oxide thickness the structure and composition of the oxide were identical for different temperatures in the range between 380 and 400°C. The high density and the low density RuO_2 thicknesses determined from XRR analysis are plotted in Fig. 2(a) as a function of annealing time for annealing temperatures of 380, 390 and 400°C. From the evolution of the high density RuO_2 thicknesses diffusion rates for oxygen diffusion in RuO_2 were determined under the reasonable assumption of diffusion limited oxide growth,[17] as follows:

$$D = \frac{dz^2}{dt}, \qquad (1)$$

where z is the HD oxide thickness and t is the annealing time. A second degree polynomial was applied to smoothen the raw data and to be able to take derivative according to Eq. 1.The calculated diffusion rates are plotted as function of HD oxide thickness in Fig. 2(b).

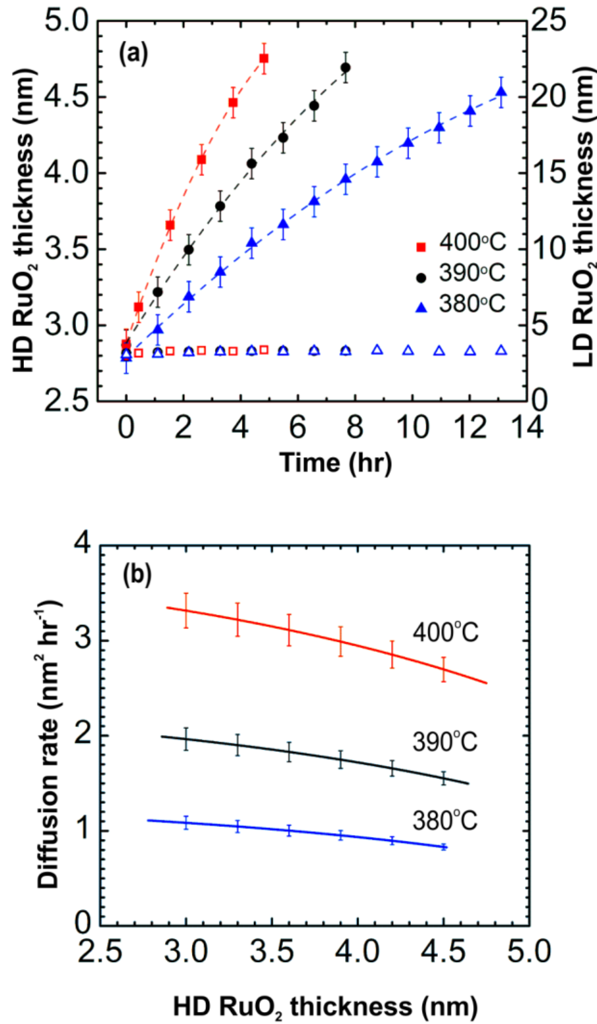

FIG. 2. (Color online) High density (HD) RuO_2 thickness (closed symbols) and low density (LD) RuO_2 thickness (open symbols) as function of annealing time (a), and diffusion rate for oxygen diffusion in RuO_2 as a function of HD RuO_2 thickness (b), for samples annealed at 380°C (triangles), 390°C (circles) and 400°C (squares). 1 $nm^2 h^{-1}$ corresponds to $2.78 \cdot 10^{-18}$ $cm^2 s^{-1}$. Dashed lines for the HD RuO_2 are guides for the eye. Note that all the samples were pre-annealed for 2 h at 400°C before *in situ* XRR measurements resulting in the initial 2.8±0.1 nm HD RuO_2 film. A second degree polynomial was applied to smoothen the raw data and to be able to take derivative according to Eq. 1 for determining the oxygen diffusion rates.

Remarkably, Fig. 2 (b) shows a general reduction of the diffusion rates with growing oxide thickness, indicating that there is a gradual change in the oxide structure with thickness that can affect diffusion. To determine oxygen diffusion kinetics and check how it depends on RuO_2 thickness, we plotted the dependence of the diffusion rates on temperature at different oxide thicknesses. In Fig. 2(b) there is a range of oxide thicknesses between 3.0 to 4.5 nm where diffusion rate data is available for all investigated temperatures. Plotting lnD versus $1/k_BT$ resulted in a linear relation for all oxide thicknesses within the explored range (Fig. 3(a)). This seems in agreement with the Arrhenius-type temperature behaviour typical for many thermally-induced processes:[17]

$$D = D_0 e^{-E_a/k_B T}, \quad lnD = lnD_0 - \frac{E_a}{k_B T}, \tag{2}$$

where D_0 is the pre-exponential factor, E_a is the activation energy, T is the absolute temperature, and k_B is the Boltzmann constant. This indicates that in spite of the reducing diffusion rates with growing oxide thickness, for every particular oxide thickness diffusion process is governed by a single diffusion mechanism with a certain activation energy. This also confirmed our initial suggestion that for each oxide thickness the structure and composition of the oxide were identical independent of what temperature was used to achieve that particular oxide thickness.

We should note that only a limited number of data points were used in this experiment to support the drawn conclusions (Fig. 3(a)). This is a result of the narrow temperature range selected in view of the peculiar growth properties of RuO_2 outside this range as described above. Nevertheless the accuracy of thickness, and especially the relative thickness change, determination with *in situ* XRR allowed us to make reliable conclusions. Fig. 3(b) shows the activation energy as a function of the growing RuO_2 thickness, determined from the slopes of the lines in Fig. 3(a).

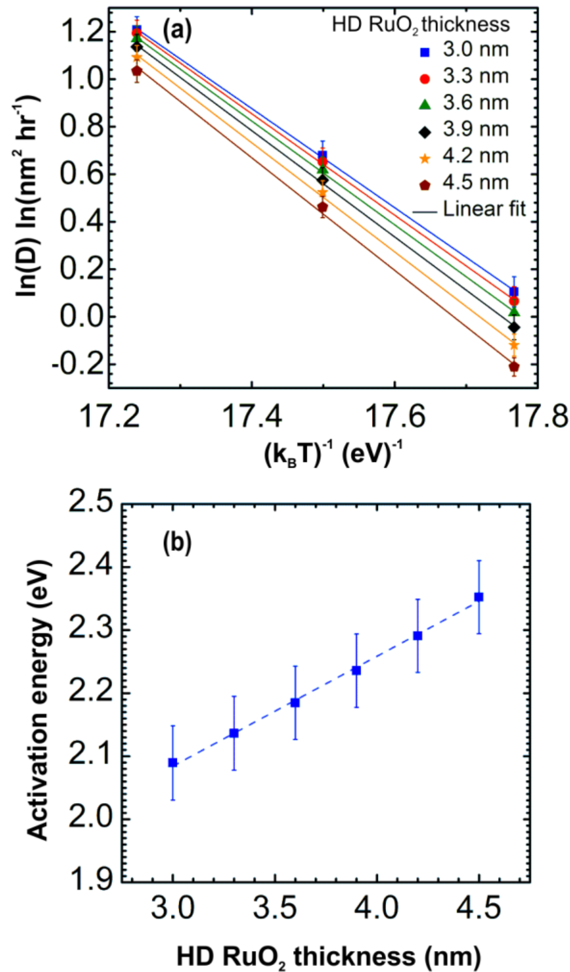

FIG. 3. (Color online) (a) Natural logarithm of the diffusion rates as a function of $1/k_BT$ for high density (HD) RuO_2 thicknesses 3.0 nm to 4.5 nm. 1 $nm^2\,h^{-1}$ corresponds to $2.78 \cdot 10^{-18}$ $cm^2\,s^{-1}$. The lines are the linear fits to the data, being in agreement with the Arrhenius equation (Eq. 2). (b) Activation energy for oxygen diffusion in RuO_2 as function of high density (HD) RuO_2 thickness. The error bars in figure (b) are the result of a systematic error for the dataset. The relative error is significantly smaller and is calculated to be below 0.05 eV. The dashed line is a guide for the eye.

The activation energy increases 2.09±0.06 to 2.35±0.06 eV while the thickness of the RuO_2 increases 3.0 to 4.5 nm. This explains the significant decrease of the diffusion rates with the growing oxide thickness. Taking into account the fact that no change in the density of the growing oxide was detected with the XRR measurements, we looked for other possible factors that could explain such significant increase in the activation energy. One of them is the crystalline structure of the formed layers.

X-ray diffraction measurements showed that Ru layer exhibited a hcp polycrystalline structure over the entire temperature range. For RuO_2, a typical pattern of a rutile-like crystalline structure was detected. The crystallite sizes of Ru and RuO_2 were determined for all temperature range using the Scherrer equation.[18] The crystal size of Ru reduced during annealing in the direction perpendicular to the sample surface. It changed from about 7.5 to 6.2 nm due to Ru consumption to form RuO_2. Opposite to Ru crystals, RuO_2 crystals showed an increase in the size. The size could not be determined accurately due to the weak diffraction signal from very thin RuO_2 film. However it was consistent with the increasing thickness of the oxide film from about 3 nm to 4.5 nm determined by X-ray reflectivity. In view of the polycrystalline structure of the layers it is very likely that diffusion in our system is dominated by the grain boundary diffusion. Usually grain boundary diffusion follows Arrhenius-type temperature dependence like lattice diffusion. So we presume that the activation energy measured in the studied system is predominantly determined by the grain boundary diffusion. If this is the case, the increase in the activation energy observed in our system should be related to the evolving grain boundary configuration in the polycrystalline RuO_2 film that could obviously occur due to the observed growth of crystallites. Nevertheless, further detailed studies are necessary to confirm this suggestion and to determine what changes in the configuration of the grain boundaries do occur.

In view of the observed change in the activation energy during annealing, it was also attractive to check the dependency of the Arrhenius pre-exponential factor on the activation energy. This dependency is observed in some systems with thermally activated processes that show Arrhenius type behaviour,[19] and recently proven not to depend on the way how the activation energy is varied.[20,21,22] The Arrhenius pre-exponential factor was calculated according to Eq. 2 for each oxide thickness. Plotting the natural logarithm of this pre-exponential factor versus the activation energy obtained for each oxide thickness resulted in a linear trend (Fig. 4). This indicates that in the studied diffusion process not only the diffusion rate depends exponentially on the activation energy, but also the pre-exponential factor is exponentially dependent on the activation energy. This suggests that the process of ruthenium oxidation at the studied stage obeys the empirical Meyer-Neldel rule (MNR),[19] which generally correlates the activation energy E_a and the logarithm of the Arrhenius pre-exponential factor D_0 as

$$lnD_0 = a + b \cdot E_a, \tag{3}$$

where a and b are constants. The 1/b value corresponds to the Meyer-Neldel energy.

In effect the increase of the pre-exponential factor when the activation energy is increased according to the Eq. 3 partially compensates for the decrease in the activation factor e^{-E_a/k_BT} in the Arrhenius equation. This can be interpreted in general terms for diffusion processes as increasing the number of paths to the activated state with the increase of the activation energy. In our experiment the effect is small compared to the effect of the activation energy on the activation factor that prevails the effect on the general diffusion rate. Still, it is significant and effectively can mean that diffusion property may depend on more than one mechanism. Further research is needed to explain physics of this phenomenon as well as see up to what thicknesses of RuO_2 the rule will still be valid. Given the sensitivity and accuracy of the used method, it is also attractive to investigate oxygen diffusion kinetics at other stages of Ru oxidation. This especially concerns the earlier stages of oxidation where only low density oxide is formed. At the advanced stages of oxidation where larger crystals are formed the lattice (volume) diffusion through RuO_2 crystals can become the limiting factor for oxygen diffusion. However in the latter case the observed deterioration of the surface morphology presents a complicating factor for the used technique.

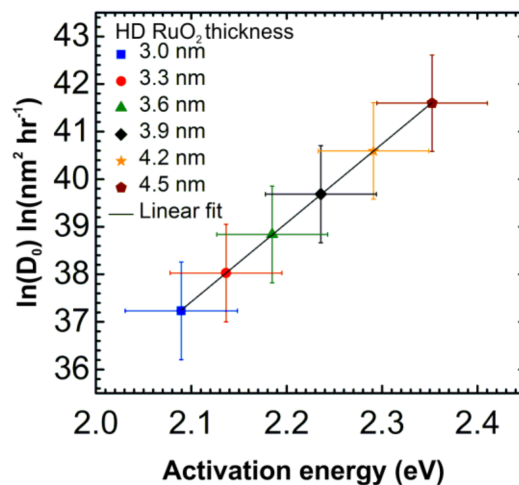

FIG. 4. (Color online) Natural logarithm of the Arrhenius pre-exponential factor as a function of the activation energy obtained for different high density RuO_2 thicknesses between 3.0 to 4.5 nm. 1 $nm^2\ h^{-1}$ corresponds to $2.78 \cdot 10^{-18}$ $cm^2\ s^{-1}$. The solid line represents the linear fit to the data according to the general Meyer-Neldel equation (Eq. 3). From the slope of the line a Meyer-Neldel energy value of 0.06±0.03 eV is obtained. Note that the error bars for the activation energies and for the pre-exponential factors represent systematic errors.

IV. CONCLUSIONS

In situ X-ray reflectivity was used to reveal diffusion kinetics of inter-diffusion process for polycrystalline ruthenium thin film oxidation. This technique allowed accurate determination of diffusion constants and activation energies for this process. It was found that diffusion rates in several nanometer thick RuO_2 films follow a linear Arrhenius dependence. However a gradual reduction in diffusion rate was observed with the growing oxide thickness. In the considered range of RuO_2 thicknesses 3.0 to 4.5 nm the activation energy for interdiffusion increased from about 2.1 to 2.4 eV. We observed no detectable change in the density of the oxide film and suggested evolving grain boundary configuration in the polycrystalline RuO_2 as a possible mechanism for the slowing interdiffusion. Further exploration revealed exponential dependence of the pre-exponential factor on the activation energy, which suggests that the process of ruthenium oxidation at the studied stage obeys the empirical Meyer-Neldel rule. And although the effect is small compared to the effect of the activation energy on the activation factor, it is significant and needs further investigation to explain physics behind this phenomenon. Also further research is needed to determine oxidation kinetics of Ru at other stages of RuO_2 formation.

ACKNOWLEDGMENTS

This work is part of the research programme 'Controlling photon and plasma induced processes at EUV optical surfaces (CP3E)' of the 'Stichting voor Fundamenteel Onderzoek der Materie (FOM)', which is financially supported by the 'Nederlandse Organisatie voor Wetenschappelijk Onderzoek (NWO)'. The CP3E programme is co-financed by Carl Zeiss SMT and ASML. We also acknowledge financial support from Agentschap NL (EXEPT project).

References:

[1] Y. Murakami, J. Li, D. Hirose, S. Kohara, and T. Shimoda, Journal of Materials Chemistry C (2015).
[2] J. H. Kim, J. H. Ahn, S. W. Kang, J. S. Roh, S. H. Kwon, and J. Y. Kim, Current Applied Physics **12**, S160 (2012).
[3] A. Krause, *Ultrathin Calcium Titanate Capacitors: Physics and Application*. (Logos Verlag Berlin, 2014).
[4] J. Jae, W. Zheng, A. M. Karim, W. Guo, R. F. Lobo, and D.G. Vlachos, ChemCatChem **6** (3), 848 (2014).
[5] E. Torun, C. M. Fang, G. A. de Wijs, and R. A. de Groot, The Journal of Physical Chemistry C **117** (12), 6353 (2013).
[6] Y. Shih, K. Lee, and Y. S. Huang, Applied Surface Science **294**, 29 (2014).
[7] H. Over, Chemical Reviews **112** (6), 3356 (2012).
[8] Q.A. Acton, *Chemical Processes—Advances in Research and Application: 2013 Edition: ScholarlyBrief*. (ScholarlyEditions, 2013).
[9] S. Wurm, in *30th European Mask and Lithography Conference* (Proc. SPIE, Dresden, Germany, 2014), Vol. 9231, pp. 923103.
[10] H. Lee, J. Choi, S. Koh, J. Kim, D. Kim, J. Choi, H. Kim, H. Ko, B. G. Kim, and C. Jeon, ECS Transactions **58** (6), 93 (2013).

[11] E. Louis, A. E. Yakshin, T. Tsarfati, and F. Bijkerk, Progress in Surface Science **86** (11-12), 255 (2011).

[12] M. Kriese, Y. Platonov, J. Rodriguez, G. Fournier, S. Grantham, C. Tarrio, J. Curry, S. Hill, and T. Lucatorto, in *Extreme Ultraviolet (EUV) Lithography VI* (Proc. SPIE, San Jose, California, United States 2015), Vol. 9422, pp. 94220K.

[13] Ho-Il Ji, Jaeyeon Hwang, Kyung Joong Yoon, Ji-Won Son, Byung-Kook Kim, Hae-Won Lee, and Jong-Ho Lee, Energy & Environmental Science **6** (1), 116 (2013).

[14] R. Coloma Ribera, R. W. E. van de Kruijs, S. Kokke, E. Zoethout, A. E. Yakshin, and F. Bijkerk, Applied Physics Letters **105** (13), 131601 (2014).

[15] R. Resel, E. Tamas, B. Sonderegger, P. Hofbauer, and J. Keckes, Journal of Applied Crystallography **36** (1), 80 (2003).

[16] M. Bjorck and G. Andersson, Journal of Applied Crystallography **40** (6), 1174 (2007).

[17] H. Mehrer, *Diffusion in Solids: Fundamentals, Methods, Materials, Diffusion-Controlled Processes*. (Springer, 2007).

[18] J. I. Langford and A. J. C. Wilson, Journal of Applied Crystallography **11** (2), 102 (1978).

[19] W. Meyer and H. Neldel, Zeitschrift für Technische Physik (Leipzig) **12**, 588 (1937).

[20] Anjani Kumar and A. Kumar, Bull Mater Sci **38** (1), 41 (2015).

[21] J. C. Palacios, M. G. Olayo, G. J. Cruz, and J. A. Chávez-Carvayar, Open Journal of Polymer Chemistry **4**, 31 (2014).

[22] K. Shimakawa and M. Aniya, Monatsh Chem **144** (1), 67 (2013).